Supplement to Contribution of Cooking Emissions to the Urban Volatile Organic Compounds in Las Vegas, NV

1 Characterizing PTR-ToF-MS Measurements of Carbonyls in Las Vegas

Long-chain carbonyls are measured by PTR-ToF-MS as the sum of isomers. Differences in isomer speciation provide evidence for varying emission sources. For example, VCP emissions from inks and coatings contain C_5 – C_7 ketones such as 2-heptanone and 4-methyl-2-pentanone (McDonald et al., 2018), while cooking emits high amounts of C_5 – C_7 aldehydes (Klein et al., 2016). VCPs emit few carbonyls with C > 7 (McDonald et al., 2018), whereas cooking is a significant source of C_8 – C_{11} aldehydes (Klein et al., 2016;Schauer et al., 1999). To determine the dominant carbonyls detected by PTR-ToF-MS in Las Vegas, GC-PTR-ToF-MS data are used to pre-separate isomers and evaluate carbonyl distributions.

Figure S1A is a GC-PTR-ToF-MS chromatogram of C_5 – C_9 carbonyls measured along the Las Vegas Strip during a nighttime drive on July 30, 2021. Each peak shows the expected proton-transfer reaction product (= VOC mass + H^+), the dehydration products that are typically observed from aliphatic aldehydes (= VOC mass + H^+ - H_2O) (Pagonis et al., 2019;Buhr et al., 2002), and additional ions that are expected from fragmentation for some molecules (e.g., octanal and nonanal). Figure S1B and S1C show chromatograms of C_8 and C_9 carbonyl standards as examples of how different carbonyls are detected by PTR-ToF-MS. The ketone isomers (e.g., 2-octanone and 2-nonanone) exhibit minimal fragmentation and are predominantly detected at the proton-transfer product at m/z 129 ($C_8H_{16}OH^+$) and m/z 143 ($C_9H_{18}OH^+$). In contrast, aldehydes mostly undergo dehydration and fragmentation, resulting in additional signals at m/z 111 ($C_8H_{15}^+$) and m/z 69 ($C_5H_8^+$) for octanal and 125 ($C_9H_{17}^+$), m/z 83 ($C_6H_{10}^+$), and m/z 69 ($C_5H_8^+$) for nonanal. Fragmentation patterns for other aldehydes are shown in Fig. S2 and compared to observations from other PTR-MS designs (Buhr et al., 2002). The proton-transfer product for aldehydes increases with carbon number, while the contribution from the dehydration product deceases as additional fragmentation results in lower carbon ions. These differences in fragmentation distinguish ketone and aldehyde isomers in GC samples.

The GC-PTR-ToF-MS chromatograms in Figure S1A show that aldehydes are the dominant carbonyls observed in the Las Vegas Strip area. Broadly, the peaks show that the fragmentation patterns observed at major carbonyl retention times agree with the expected dehydration products of aldehydes. Closer inspection of the proton-transfer products show that signals from C_5 – C_7 ketone isomers are also present in this region (likely due to VCP emissions), and therefore the proton-transfer product ions for C_5 – C_7 carbonyls (m/z 115, 101, and 87) alone cannot provide robust constraints on the spatial and temporal distribution of aldehydes in urban areas. The

dehydration products from C_5 – C_7 aldehydes (e.g., m/z 69, 83, and 97) distinguish these isomers from ketones, though it is unlikely that these ions could be used for aldehyde quantification since they are also produced from the proton-transfer of isoprene and fragmentation of cycloalkanes (Pagonis et al., 2019).

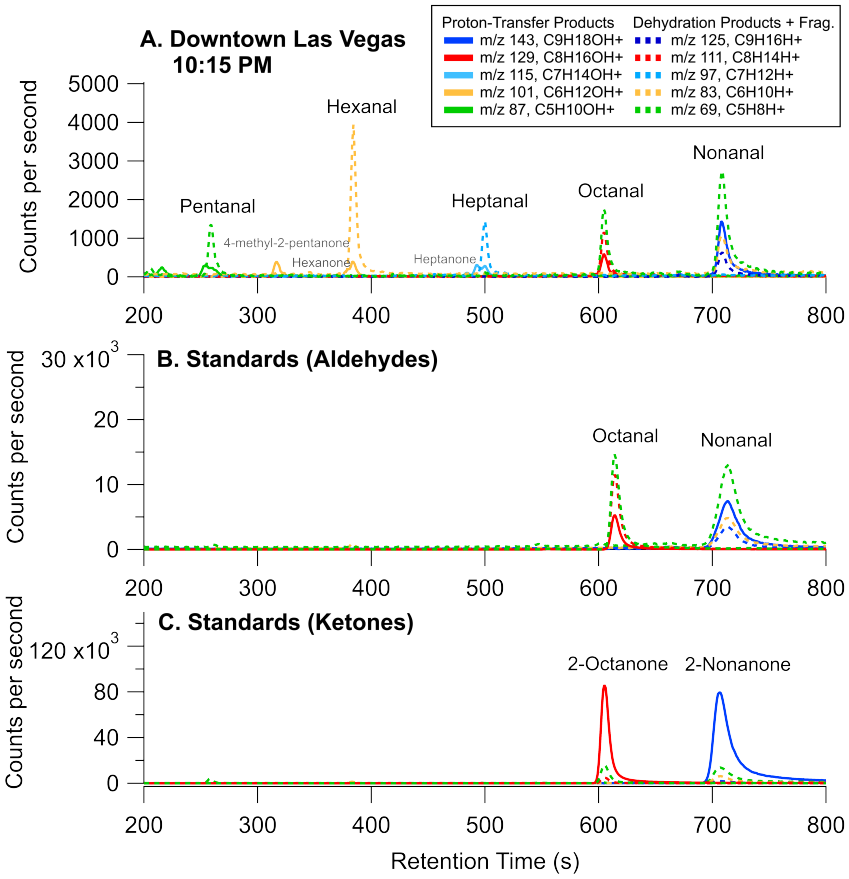

Figure S1: (A) GC-PTR-ToF-MS chromatogram showing aldehyde peaks in the Las Vegas Strip area during an evening drive on July 30, 2021. (B and C) GC-PTR-ToF-MS chromatogram of aldehyde and ketone standards and their corresponding fragmentation patterns. The peaks in the ambient chromatogram correspond to aldehydes and not ketones.

Figure S1A shows that carbonyl proton-transfer products at m/z 129 and 143 do not exhibit significant contribution from ketones isomers in the Las Vegas Strip area. The ion distribution observed from the ambient GC-PTR-ToF-MS samples agrees well with the fragmentation patterns from octanal and nonanal standards (Fig. S2B), and no additional peaks are observed in the ambient chromatogram that would suggest significant contributions to these ions from other VOCs. Therefore, m/z 129 and m/z 143 can be used to quantify octanal and nonanal without significant interferences in the Las Vegas Strip area. The proton-transfer products for octanal and nonanal are also a larger fraction of the total signal compared to smaller aldehydes (Fig. S3), which indicates that these ions are detected with higher sensitivity.

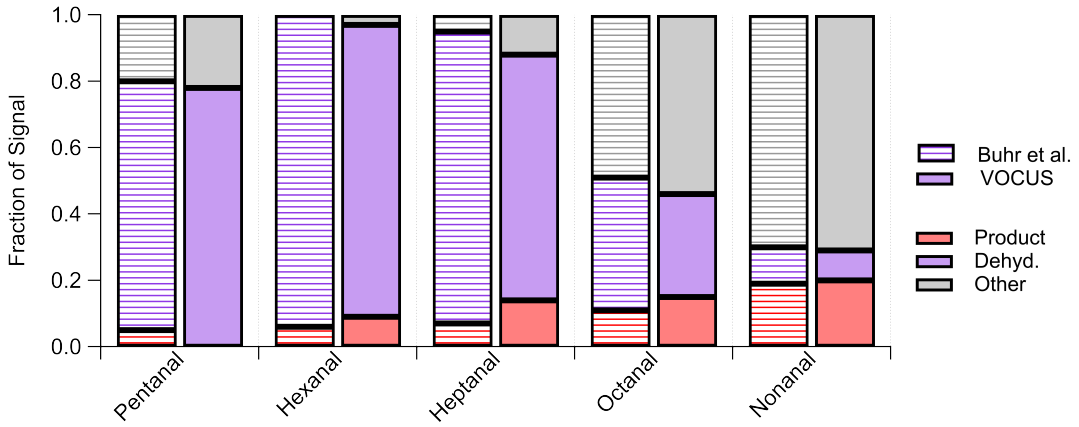

Figure S2: Distribution of ions detected by PTR-ToF-MS for C_5 – C_9 aldehydes. Solid bars represent distributions measured using a Vocus (this work) and hashed bars are distributions reported by Buhr et al. (Buhr et al., 2002). Contributions from "other" ions includes fragments and water clusters.

Mobile laboratory data also show that octanal and nonanal are the dominant carbonyl isomers throughout the Las Vegas region. Figure S3 shows PTR-ToF-MS measurements of m/z 129 and m/z 143 vs. dehydration products (m/z 125 and 111) for the entire mobile laboratory dataset. Other compounds, such as cycloalkanes, contribute to the signals at m/z 111 and 125 (Gueneron et al., 2015;Warneke et al., 2014), which explains periods when m/z 111 and 125 are elevated in the absence of m/z 129 and m/z 143. This also increases the variability in the dehydration products compared that observed for pure aldehyde standards. Most data scatter on a line that closely matches the expected fragmentation patterns for aldehydes (solid line). Furthermore, there are few data points that indicate significant contributions from ketones, which would be present as high contribution from proton-transfer products and low contributions from dehydration products (dotted line). Figures S1 and S3 demonstrate that the C_8 – C_9 carbonyls detected by PTR-ToF-MS in Las Vegas are predominantly associated with aldehydes.

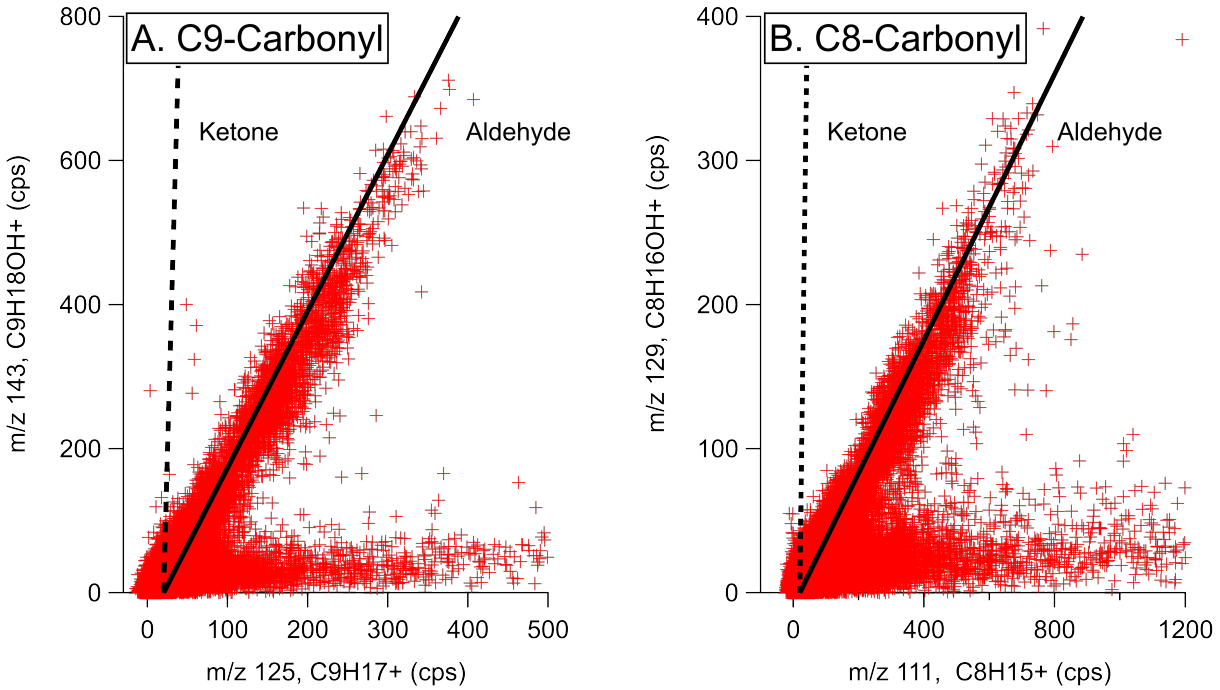

Figure S3: Mobile drive observations of (A) C_9 and (B) C_8 carbonyl proton-transfer products versus the corresponding dehydration products. The solid and dotted black lines show the aldehyde and ketone ratios from measured standards (Figure S1).

2 Corrections to masses identified as aldehydes

Figure S2 shows that C_5-C_9 aldehydes undergo significant dehydration and fragmentation reactions in PTR-ToF-MS. These compounds are among the major VOCs emitted from cooking (Klein et al., 2016;Schauer et al., 1999); consequently, corrections to these species are needed to account for the mass associated with cooking emissions. In all figures and tables, we correct aldehyde sensitivities using the carbon-dependent fragmentation patterns shown in Fig. S2. First, we determine PTR-ToF-MS sensitivities using measured or estimated proton transfer rate constants as described by Sekimoto et al. (2017). We then multiply this sensitivity by the fraction of total signal attributed to the proton-transfer rate constant of the aliphatic aldehyde with the same carbon number. For aldehydes with C > 9, we assume a fragmentation pattern that is similar to nonanal. We do not apply corrections to aldehydes with C < 5 since these compounds are not observed to fragment significantly in PTR-ToF-MS (Pagonis et al., 2019). Sensitivities for acetaldehyde, acrolein, propanal, methacrolein + crotonaldehyde, octanal, and nonanal are directly calibrated and therefore not corrected using this method.

3 Positive Matrix Factorization (PMF) Analysis

Positive matrix factorization (PMF) was conducted using the Source Finder (SoFi) software package in Igor Pro (Canonaco et al., 2013) to apportion VOCs to cooking and other urban emission sources, such as VCPs and motor vehicles. PMF is a bilinear factor model described by

Paatero (1999) and its application to ambient mass spectra is widely used and summarized elsewhere (Canonaco et al., 2013;Ulbrich et al., 2009). In short, PMF statistically apportions a matrix of data (X) into the linear combination of factor profiles (G) and temporally varying factor abundancies (F) as described by Equation 1.

$$X = GF + E \quad \text{(Eq 1)}$$

Where E is a matrix of model residuals. Inputs to the PMF algorithm include the time-varying data matrix, X, and a time-varying matrix of sample uncertainties (termed the "error matrix"). In this analysis, we evaluate the temporal behavior of 270 ions on a 10 min time basis. The error matrix reflects the uncertainty of each measurement and is calculated as two times the standard deviation of background mixing ratios.

The columns in G and the rows in F correspond to the "factors" fit by PMF to dataset X. Increasing the number of factors results in lower model residuals but can result in solutions that are non-physical. The number of factors fit to the dataset is partly chosen in order to minimize the model uncertainty to within measurement errors. The number of factors is also chosen in order to explain feasible emission sources and are justified by comparing factor profiles to molecular markers, emission fingerprints, or previously established factor profiles. In this analysis, PMF solutions were determined for 1–10 factors, but we focus on a PMF solution with 5 factors (see Section 2.2)

SoFi utilizes the multi-linear engine (ME-2) described by Paatero (1999). A key function of ME-2 is that it allows a user to input a factor profile that describes the relative distribution of VOCs associated with a given source. The degree to which this constraint is enforced in SoFi is dictated by a scalar "a-value" as described by Equation 2.

$$g_{i,solution} = g_i + a \cdot g_i \quad \text{(Eq 2)}$$

Where $g_{i,solution}$ is the factor solution resolved by PMF (G, Eq. 1), g_i is the factor profile constraint, and a is the a-value. When $a = 0$, $g_{i,solution}$ is fully constrained to g_i. Positive values allow the software to solve for $g_{i,solution}$ within uncertainty bounds dictated by the term $a \cdot g_i$. In this analysis, we constrain PMF with a mobile source profile derived from mobile measurements following the recommendations of Gkatzelis et al. (2021c) and vary a from 0.1–1 (See Section 2.1). A focus of this analysis are solutions where $a = 0.75$; however, we discuss how a 5-factor solution varies as a function of a (see Section 2.2).

3.1 Mobile Source Constraint

Previous PMF analyses on PTR-ToF-MS data in New York City (NYC) showed that resolving co-located sources can be challenging (Gkatzelis et al., 2021b). Fossil fuels were historically a dominant source of VOCs in US urban areas; however, years of regulation have resulted in major declines in fossil fuel VOC mixing ratios (Bishop and Haugen, 2018;Warneke et al., 2012). Consequently, molecules previously assigned to mobile sources, such as aromatics and ethanol, now have significant contributions from solvent sources such as paints and coatings (McDonald et al., 2018;Gkatzelis et al., 2021a;Gkatzelis et al., 2021b). For example, Figure S4 shows the time series of benzene, toluene, and the sum of C_8-aromatics measured at the Jerome Mack ground site. Benzene is often attributed to fossil fuels since it is banned from consumer products, while toluene and C_8-aromatics (e.g., xylenes) can result from both mobile sources and emissions from solvent-borne products (McDonald et al., 2018). At the Jerome Mack ground site, there are periods when aromatics correlate well (likely mobile source emissions), and there are periods when toluene and C_8-aromatics are significantly higher than benzene (likely due to a solvent source). Gkatzelis et al. (2021b) made similar observations in NYC, and it was found that an unconstrained PMF analysis resulted in a source apportionment that mixed the contributions from VCPs and mobile sources.

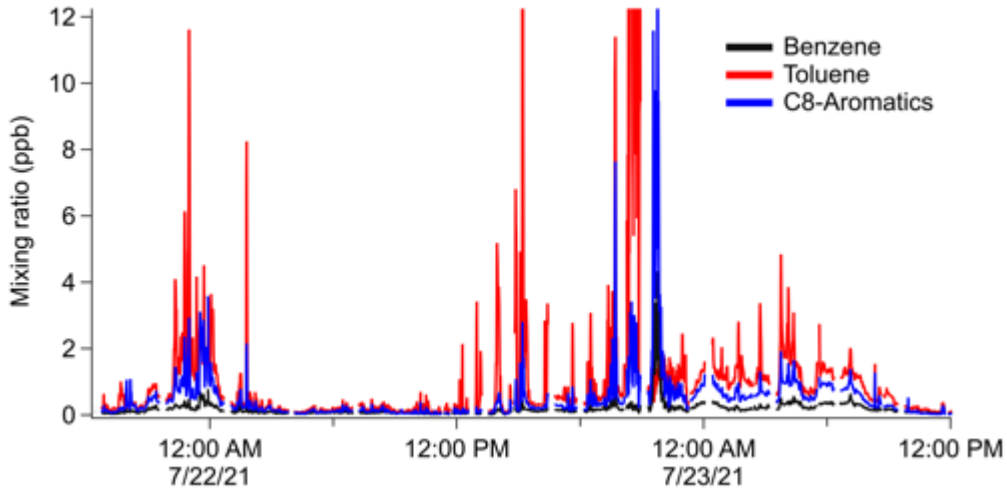

Figure S4. Time series of aromatic species measured at the Jerome Mack ground site.

To help separate mobile sources from VCPs in NYC, Gkatzelis et al. (2021b) constrained PMF with a mobile source profile that was representative of the fossil fuel emissions in the NYC area. This profile was determined using on-road VOC measurements measured by mobile laboratory, which can be used to identify and separate VOC plumes resulting from tailpipe emissions from other plumes resulting from sources such as VCPs. We follow the methods by Gkatzelis et al. (2021b) and determine a mobile source profile for Las Vegas using the mobile laboratory data collected throughout the Las Vegas Valley. Figure S5 illustrates our methods. Briefly, we identify periods when on-road mixing ratios of aromatic species, such as benzene, toluene, and C_8-aromatics, are enhanced above background mixing ratios by at least a factor of five (stringency criteria). We screen these plumes to exclude periods when VCP tracers are enhanced (e.g.,

monoterpenes, D5-siloxane). These on-road plumes must also be enriched in CO and NOx, which further differentiates mobile source enhancements of aromatics from solvent-borne emissions. We subtract out the local VOC background just outside of the plume to correct for VOCs with large regional mixing ratios (e.g., acetone, ethanol, etc.), then normalize plume-enhanced VOC mixing ratios by the total VOCs measured by PTR-ToF-MS. The mobile source profile is calculated as the average of these normalized plume profiles. In total, 100 plumes were identified and included in this analysis.

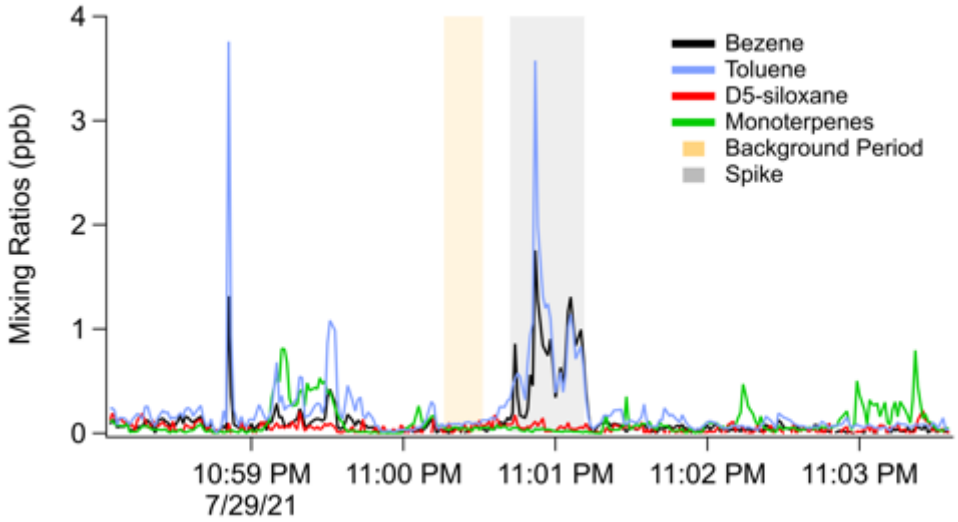

Figure S5. Mobile laboratory data showing the methods for screening for on-road mobile source emissions. Plumes are identified based on enhancements of aromatics and combustion tracers (not shown), and screened to exclude periods when VCP tracers, such as monoterpenes and D5-siloxane, are enhanced.

The resulting VOC profile is shown in Figure S6. The derived profile is very similar to the mobile fingerprint determined by Gkatzelis et al. (2021b). The profile demonstrates that ethanol is the dominant VOC from mobile sources measured by PTR-ToF-MS, followed by aromatics. Ethanol is also an important contributor to VCP emissions and therefore it is important to constrain ethanol for quantitatively apportioning VCP and mobile source emissions.

A series of sensitivity analyses were conducted to assess how the derived mobile source profile changes under different stringency criteria. Panels A, B, C, and D show sensitivity analyses when benzene is enhanced over background (BG) by varying amounts. Benzene enhancements above 2 ppb are considered “high emitters” and represent the upper 30% of all plumes identified in this analysis. Plumes averaged within the upper 74% of all emitters exhibit a similar mobile source profile as those averaged within the upper 94%. High emitters exhibit a significantly larger fraction of ethanol, but relatively similar proportion of aromatics. These results demonstrate that the fraction of ethanol in mobile source emission is likely between 0.5 – 0.6 ppb/ppb.

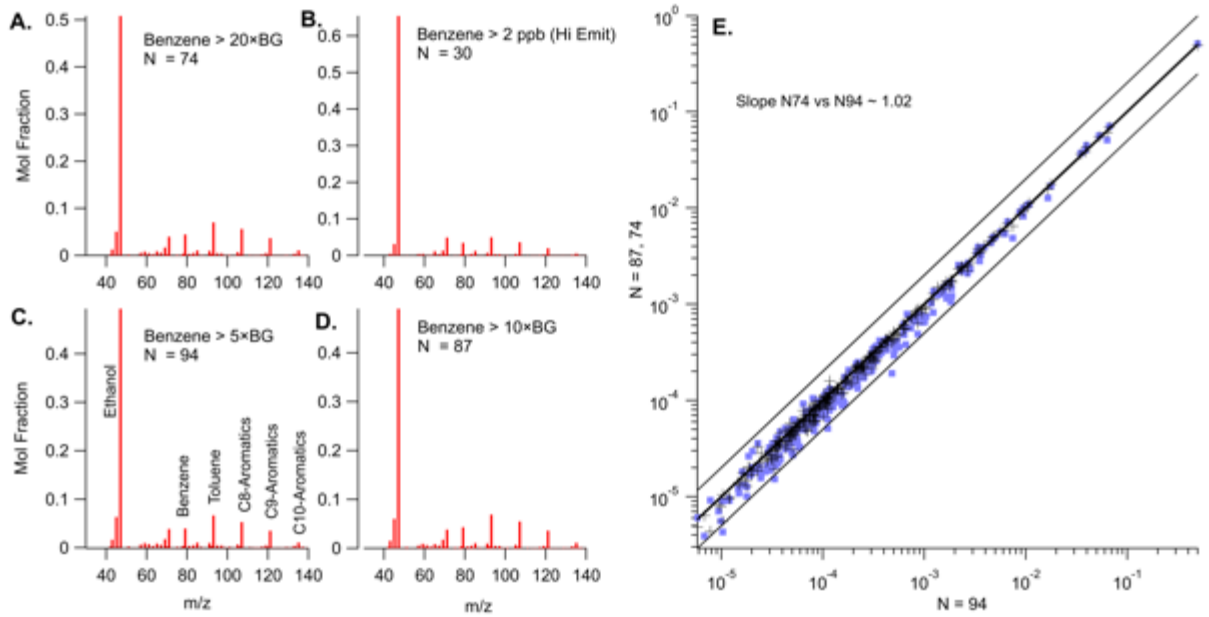

Figure S6. The derived mobile source profile based on mobile laboratory data screening processes shown in Figure 10. Panels A-D shows the derived profile under different stringency criteria, and panel E shows that screening the data to include the upper 74% of all plumes changes the derived mobile source profile by ~2 %.

3.2 PMF Results

Figures S7 and S8 show PMF results for 2 - 5 factor solutions. In all cases, the mobile source constraint is applied with an *a*-value = 0.75. Figure S9 shows the goodness-of-fit parameter, $Q/Q_{expected}$, which is the ratio of model residuals to the theoretical residuals expected for a data matrix fit to within experimental error. When $Q/Q_{expected} = 1$, the solution is considered well-fit. It is common to evaluate changes in $Q/Q_{expected}$ as additional factors are included.

For a two-factor solution, PMF attributes mass to a mobile source and all "other" sources (Figure S7). Pushing PMF to a three-factor solution results in split of the "other" category into a factor profile that peaks during the daytime, and another factor that is dominant at night. The daytime factor is primarily composed of oxygenated VOCs along with species known to be emitted or formed during daytime hours (e.g., biogenic VOCs like isoporene, methyl vinyl ketone + methacrolein, and monoterpenes). Biogenic emissions in Las Vegas are very low (< 150 ppt, Coggon et al., 2023), therefore this daytime factor is primarily composed of oxidation products (Fig. S8). The nighttime factor is largely composed of VOCs linked to primary sources (e.g., VCPs and cooking), and its diurnal pattern is primarily driven by meteorology. The nocturnal boundary layer in Las Vegas is low, but daytime heat expands the boundary layer to as high as 10 km during the day (Langford et al., 2022).

When the solution is pushed to a four-factor solution, a factor is resolved that is primarily composed of toluene and acetone with smaller contributions from xylenes and PCBTF. This factor exhibited a temporal profile characterized by brief, large enhancements in mixing ratios suggestive of a local source (Fig. 9, main text). PCBTF is a common component of solvent-borne coatings, such lacquers

and paints (Stockwell et al., 2021), and we suspect that the source is associated with a cabinet-making shop located ~300 m from the Jerome Mack ground site. We do not consider this factor representative of the regional VOC mixtures and therefore do not analyze it further.

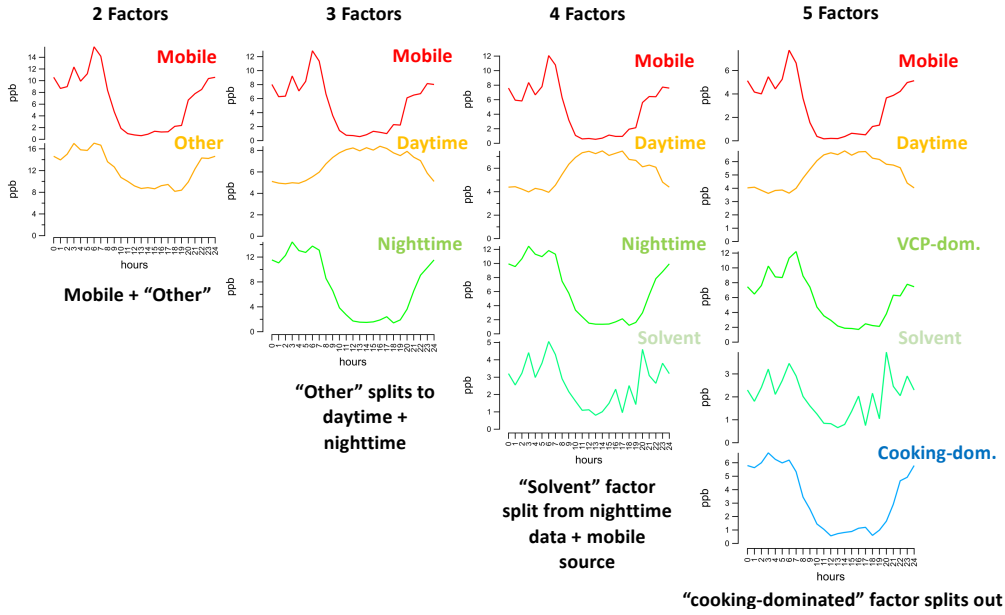

Figure S7. PMF diurnal profiles for 2 – 5 factors. Each column shows the resolved factor signal, and the description highlights the observed changes to the factor profiles.

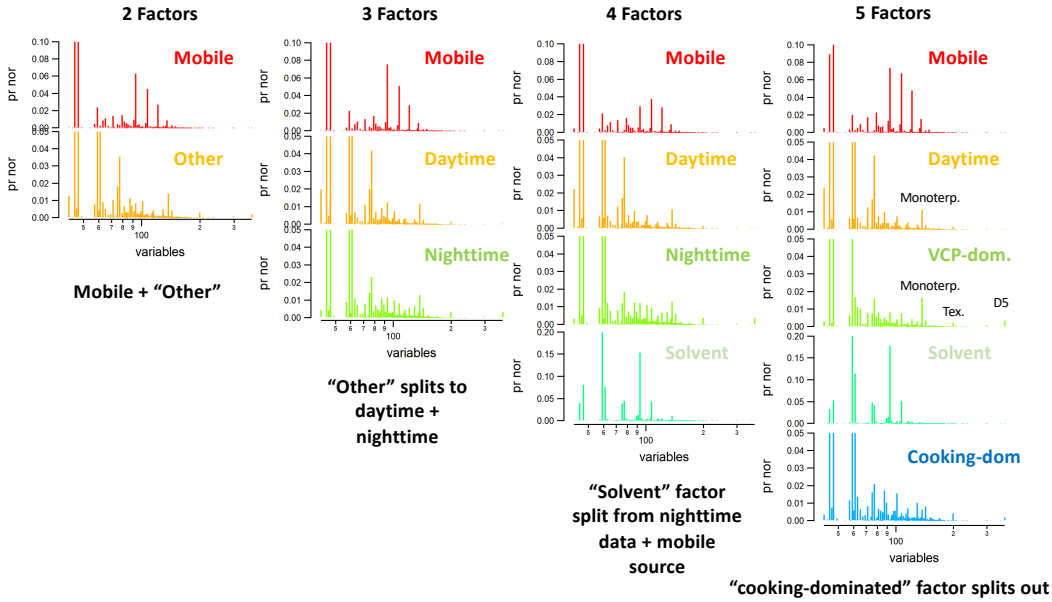

Figure S8. PMF factor profiles for 2 – 5 factors. Each column shows the resolved factor fingerprint, and the description highlights the observed changes to the factor profile.

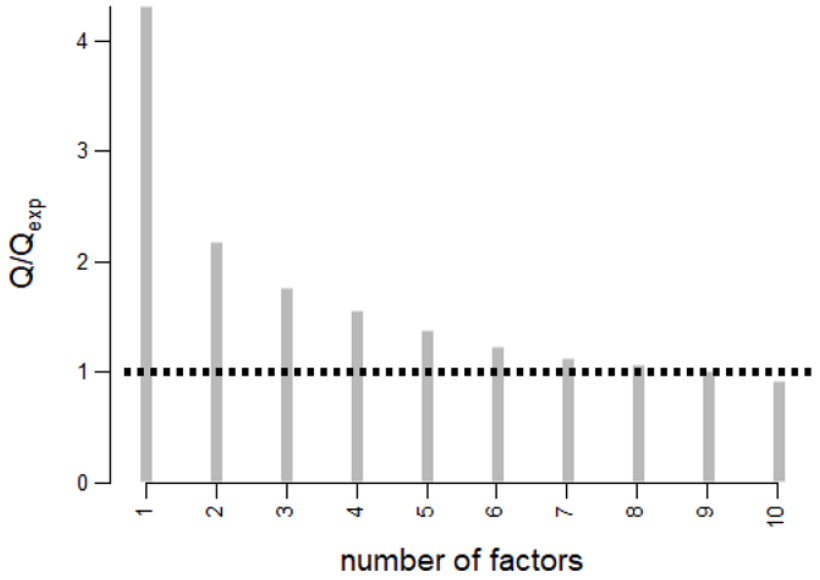

Figure S9. $Q/Q_{expected}$ for 1 – 10 factors. Increases to the factor profiles result in improved residuals

When the solution is finally pushed to five factors, PMF resolves a profile rich in aldehydes and another profile rich in ethanol, acetone, monoterpenes, and D5 These two factors are largely derived from the splitting of the nighttime and mobile source factors (Fig. S7). At 5 factors, the solution is nearly fit within the uncertainties of the measurements (Q/Q_{exp} = 1.3) and further increases in factors only result in modest improvements in residuals (Fig. S9).

The final two factors are consistent with the expected profiles for VCPs and cooking. The VCP-dominated factor is primarily composed of ethanol (EOH), but also contains D5-siloxane, monoterpenes, and acetone, which are common ingredients in consumer products. This factor resembles the VCP-dominated factor resolved in the PMF analysis for NYC described by Gkatzelis et al. (2021c). In Section 4 of the main text, we show that the mass ratio of the VCP factor to the mobile source factor closely matches the distribution represented in emissions inventories for Clark County, NV (Fig. 11). The agreement between these distributions show that a five-factor solution reasonably explains the variability of important sources in the Las Vegas region. Solutions with a smaller number of factors overestimate the contribution of mobile source emissions, while solutions with larger numbers of factors do not provide meaningful factors.

The cooking-dominated factor contains the aldehyde and acids that are shown by mobile laboratory measurements to be associated with commercial cooking emissions in Las Vegas (see Section 3.2). Figure S10 demonstrates how the factor profile resolved by PMF compares against the cooking profile measured along the Las Vegas Strip. In general, the PMF profile closely resembles the cooking profile resolved from mobile laboratory drives. There are a number of masses resolved by PMF that were not identified by the correlation analysis (e.g. ethanol, acetaldehyde, and acetone + propanal). These VOCs have significant contributions from mobile source and VCP emissions and could not be attributed to cooking by the simple correlation analysis used to determine the cooking fingerprint along the Las Vegas Strip (see Section 3.2). There are also some masses which are apportioned at lower ratios, including nonanal and heptadienal. These masses are

partially apportioned to the VCP factor, which reflects the uncertainties associated with apportioning VOCs from co-located sources. Despite these differences, the general agreement between the cooking-dominated factor and the profile determined from the Las Vegas Strip confirms that the five-factor solution effectively resolves the VOC mass associated with cooking activities. We note that the cooking profile resolved by PMF is provided in Table S1.

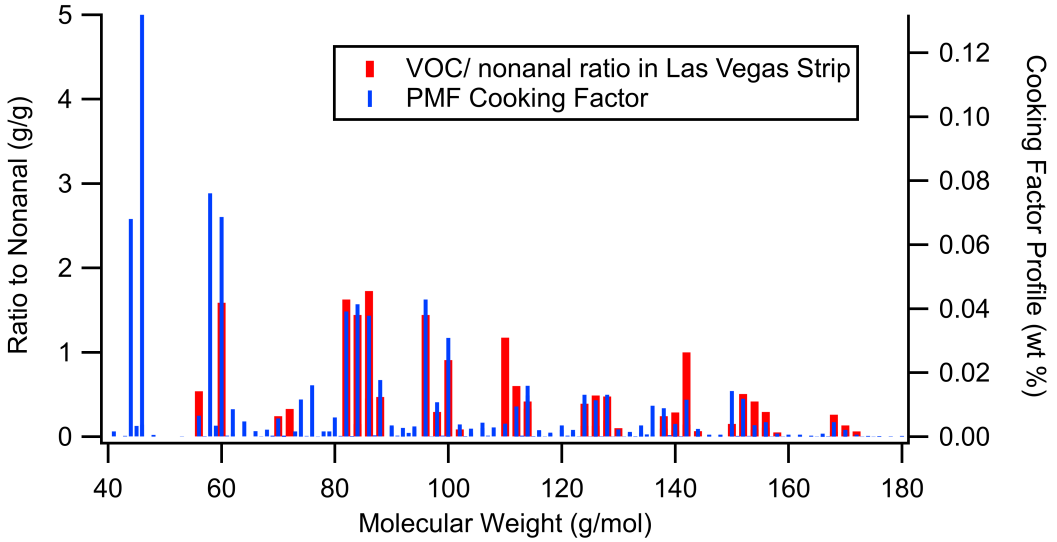

Figure S10. Comparison of the cooking-dominated factor resolved by PMF with the VOC/nonanal ratios observed along the Las Vegas Strip during mobile laboratory sampling.

Figure S11 shows how the 5-factor solution varies under different *a*-values applied to the mobile source constraint. With no constraint ($a = 1$), the mobile source factor is estimated to be ~2 times higher and the VCP-dominated factor ~4 times lower than what is resolved with more stringent constraints ($a < 1$). Similar observations were made by Gkatzelis et al. (2021c) and were associated with the overlap of VOCs that originate from both sources (e.g., ethanol, acetone, xylenes). The other factors (i.e., cooking, solvent, and daytime) show similar profiles as the solutions with $a < 1$. These results highlight the importance of applying source constraints in order to resolve VCP and mobile source emission contributions.

For solutions with $a < 1$, the profiles are similar though there is notable variability. We estimate the variability as the ratio between the standard deviation and mean calculated for all of the diurnal profiles with $a < 1$. On average, the mobile source and VCP profiles vary by 30% and 20%, respectively. This variability is reflected by changes to the PMF attribution of mass between these two sources. In contrast, the cooking, solvent, and daytime factors vary by < 7%. Consequently, while PMF variability may be highest for the mobile source and VCP factors, changes to the cooking factor are modest under different *a*-value constraints. In the main text, we present the solution for $a = 0.75$. This PMF analysis has the least constraints and provides a solution that best reflects the expected mobile source and VCP distribution represented by emissions inventories.

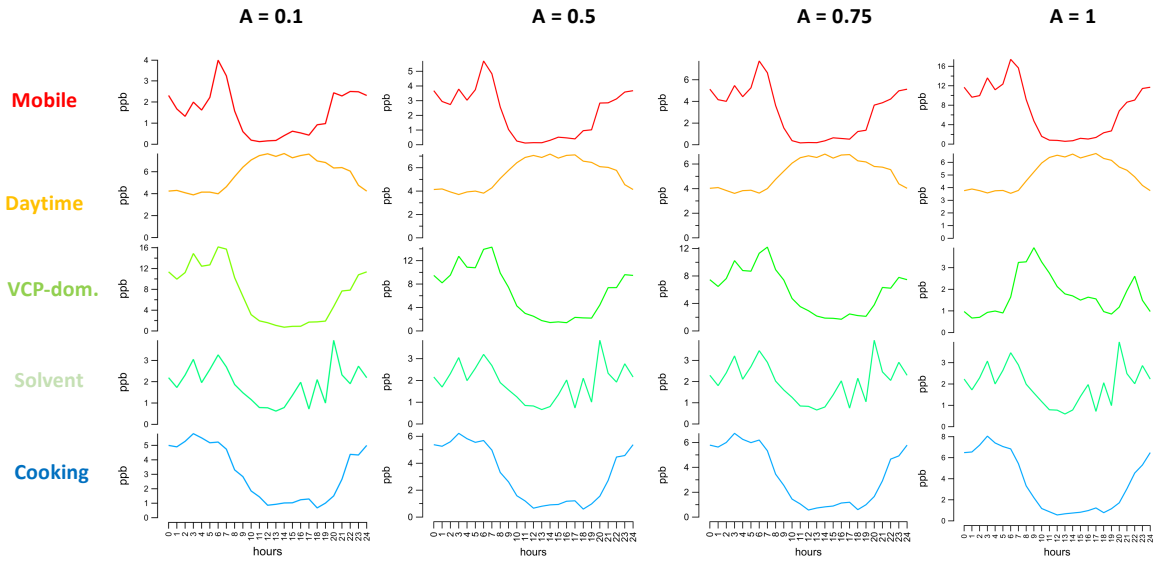

Figure S11. PMF solutions for a 5-factor system where the *a*-value applied to the mobile source constraint varies from 0.1 (highly constrained) to 1 (not constrained).

Table S1. Cooking profile resolved by PMF. Species assignments are based on the assignments provided by Klein et al. (2016).

Assigned Species	Formula	SMILES	MW (g/mol)	Class	Mass Fraction	Notes
acetaldehyde	C2H4O	CC=O	44.05	Ald	0.069	a,c
ethanol	C2H6O	CCO	46.07	Alc	0.132	a,c
acrolein	C3H4O	C=CC=O	56.06	Ald	0.007	a,c
propanal	C3H6O	CCC=O	58.08	Ald	0.076	a,c
acetic acid	C2H4O2	CC(O)=O	60.05	Acid	0.069	a,c
butenal	C4H6O	CC=CC=O	70.09	Ald	0.006	a,c
propanoic acid	C3H6O2	CCC(=O)O	74.08	Acid	0.012	a,c
pentadienal	C5H6O	C=CC=CC=O	82.1	Ald	0.039	a,c
butenedial	C4H4O2	C(=CC=O)C=O	84.07	Ald	0.004	a,c
pentenal	C5H10O	CCC=CC=O	84.12	Ald	0.041	a,c
pentanal	C5H10O	CCCCC=O	86.13	Ald	0.038	a,c
butyrolactone	C4H6O2	O=C1OCCC1	86.09	Ket	0.015	a,c
hexadienal	C6H8O	CC=CC=CC=O	96.13	Ald	0.043	a,c
pentanoic acid	C5H10O2	CCCCC(=O)O	102.13	Acid	0.004	a,c
heptadienal	C7H10O	CCC=CC=CC=O	110.15	Ald	0.004	a,c
heptenal	C7H12O	CCCCC=CC=O	112.17	Ald	0.009	a,c
heptanal	C7H14O	CCCCCCC=O	114.19	Ald	0.013	a,c
octadienal	C8H12O	CCCC=CC=CC=O	124.18	Ald	0.013	a,c
octenal	C8H14O	CCCCCC=CC=O	126.2	Ald	0.011	a,c
octanal	C8H16O	CCCCCCCC=O	128.21	Ald	0.013	a,c
heptanoic acid	C7H14O2	CCCCCCC(=O)O	130.18	Acid	0.001	a,c

monoterpene	C10H16	---	136.23	Terp	0.010	a,c
nonadienal	C9H14O	CCCCC=CC=CC=O	138.21	Ald	0.009	a,c
nonenal	C9H16O	CCCCCCC=CC=O	140.22	Ald	0.004	a,c
nonanal	C9H18O	CCCCCCCCC=O	142.24	Ald	0.012	a,c
octanoic acid	C8H16O2	CCCCCCCC(=O)O	144.21	Acid	0.002	a,c
decatrienal	C10H14O	CCCC=CC=CC=CC=O	150.22	Ald	0.014	b,c
decadienal	C10H16O	CCCCCC=CC=CC=O	152.23	Ald	0.012	a,c
decenal	C10H18O	CCCCCCCC=CC=O	154.25	Ald	0.004	a,c
decanal	C10H20O	CCCCCCCCCC=O	156.26	Ald	0.004	a,c
nonanoic acid	C9H18O2	CCCCCCCCC(=O)O	158.24	Acid	0.001	a,c
undecenal	C11H22O	CCCCCCCCC=CC=O	168.28	Ald	0.001	a,c
undecanal	C11H20O	CCCCCCCCCC=O	170.29	Ald	0.002	a,c
decenoic acid	C10H18O2	CCCCCCCC=CC(=O)O	170.25	Acid	0.002	b,c
decanoic acid	C10H20O2	CCCCCCCCCC(=O)O	172.26	Acid	0.001	a,c
tridecanal	C13H26O	CCCCCCCCCCCCC=O	198.34	Ald	0.002	a,c
Total					***0.70***	
Other Masses (lower certainty)						
furfural	C5H4O2	C1=COC(=C1)C=O	96.08	Ald	0.005	b,c
C7H8O2	C7H8O2	---	124.14	Acid	0.005	c
benzaldehyde	C7H6O	C1=CC=C(C=C1)C=O	106.12	Ald	0.004	a,c
C6H8O2	C6H8O2	---	112.13	Acid	0.004	c
C6H10O2	C6H10O2	---	114.14	Acid	0.016	c
C8H1002	C8H1002	---	138.16	Acid	0.003	c
C8H12O2	C8H12O2	---	140.18	Acid	0.003	c
C8H14O2	C8H14O2	---	142.2	Acid	0.006	c
C9H14O2	C9H14O2	---	154.21	Acid	0.002	c
C9H16O2	C9H16O2	---	156.22	Acid	0.002	c
Total					***0.05***	
Unspeciated					***0.25***	

[a] isomer identity based on identity reported by Klein et al. (2016)
[b] assumed isomer identity
[c] compound class based on assignments given by Klein et al. (2016)

3.3 Supplemental Figures to the Main Text

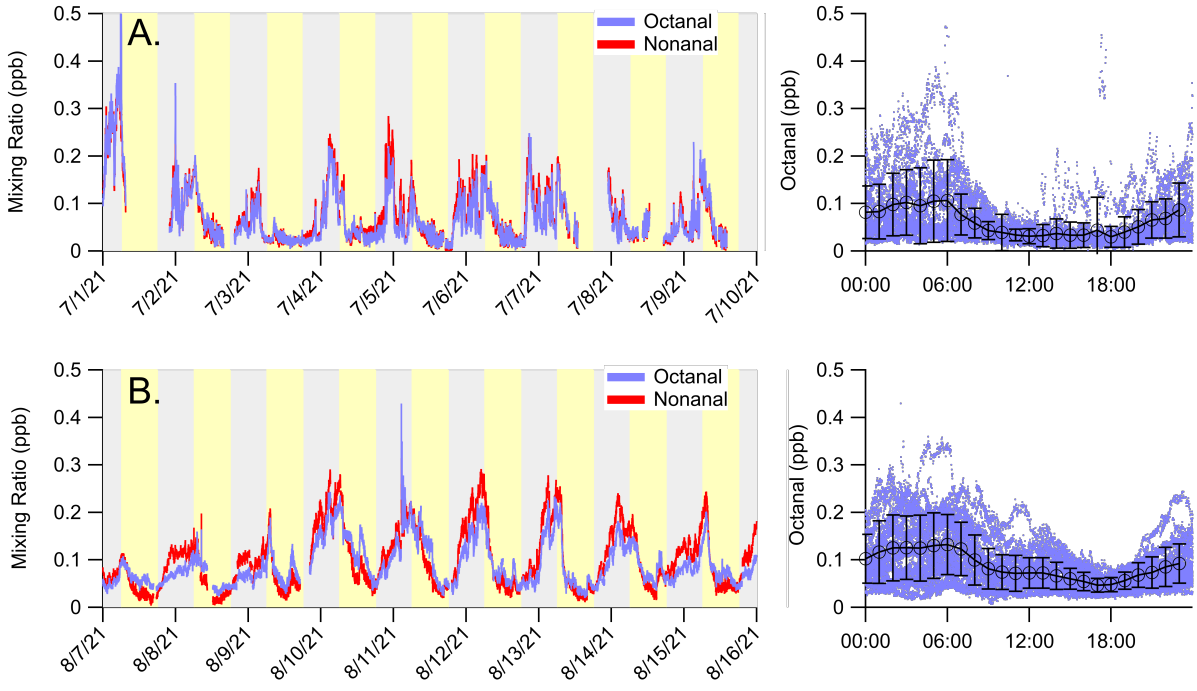

Figure S12: Time series and diurnal pattern of octanal and nonanal in (A) Las Vegas, NV and (B) Pasadena, CA. Yellow and grey backgrounds indicate measurements conducted during the day (6:00 AM – 6:00 PM local time) and night (6;00 PM – 6:00 AM), respectively.

References

Bishop, G. A., and Haugen, M. J.: The Story of Ever Diminishing Vehicle Tailpipe Emissions as Observed in the Chicago, Illinois Area, Environ. Sci. Technol., 52, 7587-7593, 10.1021/acs.est.8b00926, 2018.

Buhr, K., van Ruth, S., and Delahunty, C.: Analysis of volatile flavour compounds by Proton Transfer Reaction-Mass Spectrometry: fragmentation patterns and discrimination between isobaric and isomeric compounds, International Journal of Mass Spectrometry, 221, 1-7, https://doi.org/10.1016/S1387-3806(02)00896-5, 2002.

Canonaco, F., Crippa, M., Slowik, J. G., Baltensperger, U., and Prévôt, A. S. H.: SoFi, an IGOR-based interface for the efficient use of the generalized multilinear engine (ME-2) for the source apportionment: ME-2 application to aerosol mass spectrometer data, Atmos. Meas. Tech., 6, 3649-3661, 10.5194/amt-6-3649-2013, 2013.

Coggon, M. M., Stockwell, C. E., Claflin, M. S., Pfannerstill, E. Y., Lu, X., Gilman, J. B., Marcantonio, J., Cao, C., Bates, K., Gkatzelis, G. I., Lamplugh, A., Katz, E. F., Arata, C., Apel, E. C., Hornbrook, R. S., Piel, F., Majluf, F., Blake, D. R., Wisthaler, A., Canagaratna, M., Lerner, B. M., Goldstein, A. H., Mak, J. E., and Warneke, C.: Identifying and correcting interferences to

PTR-ToF-MS measurements of isoprene and other urban volatile organic compounds, EGUsphere, 2023, 1-41, 10.5194/egusphere-2023-1497, 2023.

Gkatzelis, G. I., Coggon, M. M., McDonald, B. C., Peischl, J., Aikin, K. C., Gilman, J. B., Trainer, M., and Warneke, C.: Identifying Volatile Chemical Product Tracer Compounds in US Cities, Environ. Sci. Technol., 55, 188-199, 10.1021/acs.est.0c05467, 2021a.

Gkatzelis, G. I., Coggon, M. M., McDonald, B. C., Peischl, J., Gilman, J. B., Aikin, K. C., Robinson, M. A., Canonaco, F., Prevot, A. S. H., Trainer, M., and Warneke, C.: Observations Confirm that Volatile Chemical Products Are a Major Source of Petrochemical Emissions in US Cities, Environ. Sci. Technol., 55, 4332-4343, 10.1021/acs.est.0c05471, 2021b.

Gkatzelis, G. I., Coggon, M. M., McDonald, B. C., Peischl, J., Gilman, J. B., Aikin, K. C., Robinson, M. A., Canonaco, F., Prevot, A. S. H., Trainer, M., and Warneke, C.: Observations Confirm that Volatile Chemical Products Are a Major Source of Petrochemical Emissions in U.S. Cities, Environmental Science & Technology, 55, 4332-4343, 10.1021/acs.est.0c05471, 2021c.

Gueneron, M., Erickson, M. H., VanderSchelden, G. S., and Jobson, B. T.: PTR-MS fragmentation patterns of gasoline hydrocarbons, International Journal of Mass Spectrometry, 379, 97-109, https://doi.org/10.1016/j.ijms.2015.01.001, 2015.

Klein, F., Platt, S. M., Farren, N. J., Detournay, A., Bruns, E. A., Bozzetti, C., Daellenbach, K. R., Kilic, D., Kumar, N. K., Pieber, S. M., Slowik, J. G., Temime-Roussel, B., Marchand, N., Hamilton, J. F., Baltensperger, U., Prévôt, A. S. H., and El Haddad, I.: Characterization of Gas-Phase Organics Using Proton Transfer Reaction Time-of-Flight Mass Spectrometry: Cooking Emissions, Environmental Science & Technology, 50, 1243-1250, 10.1021/acs.est.5b04618, 2016.

Langford, A. O., Senff, C. J., Alvarez Ii, R. J., Aikin, K. C., Baidar, S., Bonin, T. A., Brewer, W. A., Brioude, J., Brown, S. S., Burley, J. D., Caputi, D. J., Conley, S. A., Cullis, P. D., Decker, Z. C. J., Evan, S., Kirgis, G., Lin, M., Pagowski, M., Peischl, J., Petropavlovskikh, I., Pierce, R. B., Ryerson, T. B., Sandberg, S. P., Sterling, C. W., Weickmann, A. M., and Zhang, L.: The Fires, Asian, and Stratospheric Transport–Las Vegas Ozone Study (FAST-LVOS), Atmos. Chem. Phys., 22, 1707-1737, 10.5194/acp-22-1707-2022, 2022.

McDonald, B. C., de Gouw, J. A., Gilman, J. B., Jathar, S. H., Akherati, A., Cappa, C. D., Jimenez, J. L., Lee-Taylor, J., Hayes, P. L., McKeen, S. A., Cui, Y. Y., Kim, S. W., Gentner, D. R., Isaacman-VanWertz, G., Goldstein, A. H., Harley, R. A., Frost, G. J., Roberts, J. M., Ryerson, T. B., and Trainer, M.: Volatile chemical products emerging as largest petrochemical source of urban organic emissions, Science, 359, 760-764, 10.1126/science.aaq0524, 2018.

Paatero, P.: The Multilinear Engine—A Table-Driven, Least Squares Program for Solving Multilinear Problems, Including the n-Way Parallel Factor Analysis Model, Journal of Computational and Graphical Statistics, 8, 854-888, 10.1080/10618600.1999.10474853, 1999.

Pagonis, D., Sekimoto, K., and de Gouw, J.: A Library of Proton-Transfer Reactions of H3O+ Ions Used for Trace Gas Detection, Journal of The American Society for Mass Spectrometry, 30, 1330-1335, 10.1007/s13361-019-02209-3, 2019.

Schauer, J. J., Kleeman, M. J., Cass, G. R., and Simoneit, B. R. T.: Measurement of Emissions from Air Pollution Sources. 1. C1 through C29 Organic Compounds from Meat Charbroiling, Environmental Science & Technology, 33, 1566-1577, 10.1021/es980076j, 1999.

Sekimoto, K., Li, S.-M., Yuan, B., Koss, A., Coggon, M., Warneke, C., and de Gouw, J.: Calculation of the sensitivity of proton-transfer-reaction mass spectrometry (PTR-MS) for organic trace gases using molecular properties, International Journal of Mass Spectrometry, 421, 71-94, https://doi.org/10.1016/j.ijms.2017.04.006, 2017.

Stockwell, C. E., Coggon, M. M., Gkatzelis, G. I., Ortega, J., McDonald, B. C., Peischl, J., Aikin, K., Gilman, J. B., Trainer, M., and Warneke, C.: Volatile organic compound emissions from solvent- and water-borne coatings – compositional differences and tracer compound identifications, Atmos. Chem. Phys., 21, 6005-6022, 10.5194/acp-21-6005-2021, 2021.

Ulbrich, I. M., Canagaratna, M. R., Zhang, Q., Worsnop, D. R., and Jimenez, J. L.: Interpretation of organic components from Positive Matrix Factorization of aerosol mass spectrometric data, Atmos. Chem. Phys., 9, 2891-2918, 10.5194/acp-9-2891-2009, 2009.

Warneke, C., de Gouw, J. A., Holloway, J. S., Peischl, J., Ryerson, T. B., Atlas, E., Blake, D., Trainer, M., and Parrish, D. D.: Multiyear trends in volatile organic compounds in Los Angeles, California: Five decades of decreasing emissions, J. Geophs. Res., 117, 1-10, 10.1029/2012jd017899, 2012.

Warneke, C., Geiger, F., Edwards, P. M., Dube, W., Pétron, G., Kofler, J., Zahn, A., Brown, S. S., Graus, M., Gilman, J. B., Lerner, B. M., Peischl, J., Ryerson, T. B., de Gouw, J. A., and Roberts, J. M.: Volatile organic compound emissions from the oil and natural gas industry in the Uintah Basin, Utah: oil and gas well pad emissions compared to ambient air composition, Atmos. Chem. Phys., 14, 10977-10988, 10.5194/acp-14-10977-2014, 2014.